applied sciences

MDPI

*Article*

# Light-Induced Ring Pattern in a Dye-Doped Nematic Liquid Crystal

**Marcel G. Clerc [1,*], Gregorio González-Cortés [1], Paulina I. Hidalgo [2], Lucciano A. Letelier [1], Mauricio J. Morel [3] and Jorge Vergara [2]**

[1] Departamento de Física and Millennium Institute for Research in Optics, Facultad de Ciencias Físicas y Matemáticas, Universidad de Chile, Casilla 487-3, Santiago 851, Chile; gregorio.gonzalez@ug.uchile.cl (G.G.-C.); lucciano.letelier@ug.uchile.cl (L.A.L.)
[2] Departamento de Química Orgánica, Facultad de Ciencias Químicas, Universidad de Concepción, Concepción 129, Chile; pauhidal@udec.cl (P.I.H.); jovergar@udec.cl (J.V.)
[3] Departamento de Química y Biología, Facultad de Ciencias Naturales, Universidad de Atacama, Ave. Copayapu, Copiapó 485, Chile; mauricio.morel@uda.cl
* Correspondence: marcel@dfi.uchile.cl; Tel.: +56-2-29784676

**Abstract:** The use of dye-doped liquid crystals allows the amplification of the coupling of light and liquid crystals. Light can induce the self-organization of the molecular order. The appearance of ring patterns has been observed, which has been associated with phase modulation. However, the morphology and dynamics of the ring patterns are not consistent with self-modulation. Based on an experimental setup with two parallel coherence beams orthogonal to a liquid crystal cell, one of which induces photo-isomerization and the other causes illumination, the formation of ring patterns is studied. To use these two coherent beams, we synthesize methylred methyl ester as a dye-dopant, which is photosensitive only to one of the light beams, and a commercial E7 liquid crystal as a matrix. Based on a mathematical model that accounts for the coupling between the concentration of the *cis*-state and the order parameter, we elucidate the emergence of the rings as forming patterns in an inhomogeneous medium. The bifurcation diagram is analytically characterized. The emergence, propagation of the rings, and the establishment of the ring patterns are in fair agreement with the experimental observations.

**Keywords:** photo-isomerization in liquid crystals; pattern formation; light-induced phenomena; azo-dye-dopant



**Citation:** Clerc, M.G.; González-Cortés, G.; Hidalgo, P.I.; Letelier, L.A.; Morel, M.J.; Vergara, J. Light-Induced Ring Pattern in a Dye-Doped Nematic Liquid Crystal. *Appl. Sci.* **2021**, *11*, 5285. https://doi.org/10.3390/app11115285

Academic Editor: Gaetano Assanto

Received: 14 May 2021
Accepted: 1 June 2021
Published: 7 June 2021



## 1. Introduction

The interaction between light and matter has played a fundamental role in the understanding and characterization from the early stages of research [1]. Likewise, the interaction between light and matter has also been the basis of the development of technological elements such as mirrors, lenses, telescopes, microscopes, lasers, and waveguides, among others. The development of more coherent and monochromatic light sources (lasers) accompanied by materials that present stronger nonlinear responses has allowed the creation of a great variety of devices [2–6]. Liquid crystals are one of the most versatile materials, because of their strong nonlinear response and reorientation capacity through the application of electromagnetic waves and electric and magnetic fields [7–11]. Liquid crystals are a state of matter in which the molecules have a preferential orientation and can have or not have a positional order; this organization is also known as soft matter [7–11]. Indeed, this state of matter shares features of solids and liquids. In particular, fluidity, molecular reorientation, and birefringence are characteristic properties of liquid crystals. One of the most studied types of liquid crystals used in technological applications are nematic liquid crystals (NLC). This state is composed of rod-like organic molecules [7–11]. Because of an intermolecular interaction, these molecules are arranged to have a similar molecular

orientation without positional order for specific temperature ranges. This results in a sharp anisotropy of all their physical properties, especially regarding elastic and optical characteristics. Likewise, the ability to reorient the molecular order has allowed the development of many applications, mainly liquid crystal displays (LCDs) and sensors [12]. The LCD is perhaps the best known liquid crystal application by the public today. However, in most of these applications, the control of molecular reorientation is done through electric fields. LCDs therefore require transparent or reflective electrodes, power sources, and other elements. Another manner of achieving molecular reorientation is to consider the application of electromagnetic waves through the liquid crystal sample [13–17]. However, this type of strategy requires the use of strong electromagnetic fields, which typically need a power on the order of 100 W/cm$^2$. For these powers, the nonlinear response of the medium is activated [11,18]. The previous scenario can change radically when one considers the dye-dopant inside the liquid crystal matrix. Indeed, when nematics are doped with azo-dyes, their nonlinear response to opto-electrical perturbations is increased by several orders of magnitude [11,18]. Indeed, azo-dyes mediate the origin of the coupling of the electromagnetic waves with the liquid crystal; when these molecules are irradiated, they present an isomeric transition. This phenomenon is known as the Jánossy effect [19]. This transition is characterized by the fact that the molecule changes from an elongated structure (*trans*-state) to one with a boomerang shape (*cis*-state) when the molecule absorbs a photon. Figure 1 illustrates the typical structure of these molecules.

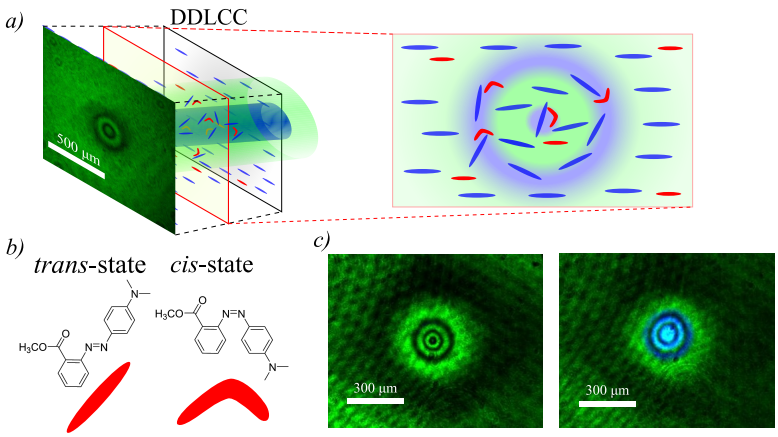


**Figure 1.** Ring patterns induced by light in a dye-doped liquid crystal cell (DDLCC). (**a**) Schematic representation of the experimental system. The blue and red bars, respectively, account for the molecules of the liquid crystal and azo-dye. The cell is illuminated by a blue and green beam. The snapshot accounts for the observed ring patterns. A transversal plane in the DDLCC is schematically represented. The areas under higher blue laser irradiation are more disordered, while the zones less illuminated preserve the nematic order. (**b**) Isomers of the molecule methyl red methyl ester. (**c**) Two snapshots showing the observed pattern (upper panel) and snapshot with the beam that induces photo-isomerization superimposed (bottom panel).

When a sufficiently intense light beam illuminates a thin film of dye-doped nematic liquid crystal, this can induce molecular disorder, generating a transition from a nematic phase to an isotropic one [20]. This type of transition is characterized by the emergence of a front between phases [20]. These fronts are characterized by being a circular spot that gathers in the center of the beam and spreads outwards and stops in the region where both states are energetically equivalent, Maxwell point. For intermediate light intensities, which do not induce isotropic liquid phase, the emergence of a pattern with a stripe shape has been reported [21,22]. In fact, these patterns correspond to regions that alternate higher and lower orientational molecular order. This phenomenon is understood as a result of the different scales in the transport processes of the concentration of the *cis* state and the orientational order of the liquid crystal. Thin films of liquid crystals without dye-

dopants subjected to strong electromagnetic fields in their cross section exhibit diffraction rings [14,23]. The above phenomenon is associated with phase modulation or autofocusing of light when is diffracted in the NLC. This medium is a good approximation to a Kerr medium [2–6,24], that is, the envelope of the light is under the effect of phase modulation, a cubic term for the envelope and diffraction. Hence, the conjunction of diffraction and phase modulation produces the emergence of diffraction rings. Note that the thickness of the observed rings decreases with the square distance from the center of the light beam. A similar phenomenon is observed in dye-doped liquid crystals when subjected to a coherent light with a moderate and low light intensity [25–27]. Because of the presence of dye-dopants, the nonlinear response can be achieved for light power of a few milliwatts [28]. The emergence of these rings has been associated with phase modulation. However, the morphology and dynamics of the ring patterns are not consistent with that expected for self-modulation rings observed for large intensities of light [14,23]. Furthermore, in this type of description, the dynamical behavior of the *cis* state concentration is passive. In other words, this concentration is enslaved to the system dynamics.

The article aims to elucidate and characterize the origin of the ring patterns observed when illuminating a dye-doped nematic liquid crystal cell with a light beam and planar anchoring. Based on an experimental setup with two parallel coherent beams, one of which induces photo-isomerization and the other the illumination, the formation of ring patterns is studied. Figure 1 illustrates the typical observed ring patterns. This type of setup allows us to separate the induction of the photo-isomerization and the observation of the self-organized patterns. To use these two coherent beams, we have synthesized methyl red methyl ester as dye-dopant, photo sensitive only to one of the light beams, and a commercial E7 (Instec Inc., Boulder, CO, USA) as a liquid crystal matrix. The methylred methyl ester was used as a dye-dopant (cf. Figure 1). Unlike methylred, the methylred methyl ester is more soluble and less viscous in E7 due to the absence of hydrogen bonds from the carboxylic acid group of the methylred. In addition, this structural modification prevents an intramolecular hydrogen bonding interaction with one of the nitrogens of the azo group, causing a faster *cis-trans* isomerization [29]. Theoretically, based on a mathematical model that accounts for the coupling between the concentration of the *cis* state and the order parameter, we elucidate the emergence of the rings as forming patterns in an inhomogeneous medium. The bifurcation diagram is analytically characterized. The emergence, propagation, and establishment of the ring patterns are in fair agreement with the experimental observations.

## 2. Experimental Observations of the Ring Patterns

The conventional phototropic transition detection is performed by sampling the excitation laser beam and extracting the reorientational order parameter with polarized optical microscopy [19–23,30]. The main inconvenience with those setups arises from the loss of information of the liquid crystal dynamics outside of the central Gaussian illuminated zone. Hence, the impossibility of differentiating between polarization changes in the light filtered out by the analyzer and the absorbed light by the sample. To overcome these difficulties, we developed an experimental setup with two parallel coherent beams applied to the dye-doped liquid crystal sample, which is only photo-sensitive to one beam (excitation beam) while the other is harmless (probing beam).

### 2.1. Experimental Setup

Figure 2 shows the experimental setup diagram. The dye-doped liquid crystal cell (DDLCC) undergoes a phototropic transition when it is irradiated by a light source in the absorption band of the guest dye [19,31]. We used a concentration of methylred methyl ester 1 wt% as azo-dye guest doping a commercially available E7 NLC (host). The chemical structure and isomers of methylred methyl ester are illustrated in Figure 1c. The absorption spectrum of the methylred methyl ester is depicted in Figure 2b (for details about the chemical synthesis and depuration of the azo-colorant, see Section 2.2).

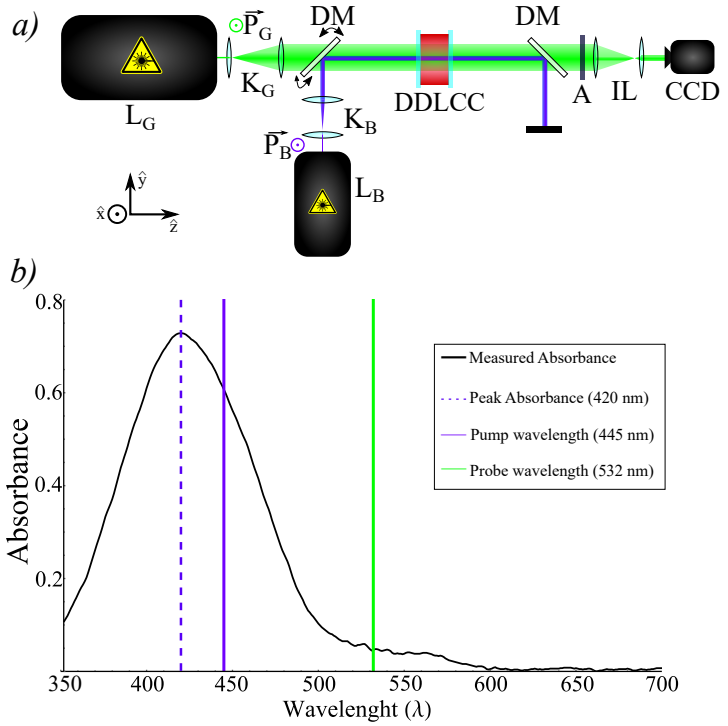


**Figure 2.** Experimental setup for the dye-doped nematic liquid crystal phototropic transition with a harmless external illumination. (**a**) A dye-doped liquid crystal cell (DDLCC) is irradiated by a 445 nm blue laser (excitation light beam) $L_B$ and illuminated by a 532 nm green laser (probing light beam) $L_G$. Two pairs of lenses are placed in a Kepler telescope configuration $K_B$ and $K_G$ to expand the laser beam while preserving the collimation. $\vec{P}_B$ and $\vec{P}_G$ are the polarization of the laser sources. A long-wave pass dichroic mirror $DM$ is used to set both excitation and probing on the same optical line. After the DDLCC, another long-wave pass dichroic mirror is used to filter out the excitation beam. An analyzer in a crossed configuration with respect to $\vec{P}_G$. A set of imaging optics $IL$ consisting on a $\times 2$ Kepler telescope and a $\times 7$ zoom lens is used to enhance the image captured by the $1/2''$ CCD camera. (**b**) Absorption spectrum of methyl red methyl ester in dichloromethane $2.0 \times 10^{-5}$ mol/L. The solid vertical lines account for the wavelength of the exciting and probing light, respectively. Vertical dashed lines account for the absorption maximum.

The mixture was injected into an antiparallel planarly aligned liquid crystal cell with a thickness of 25 µm (Instec Inc., Boulder, CO, USA). A 445 nm Cobolt 90 nW Polarized Laser was used as an exciting irradiation source to generate a phototropic transition. The polarization $\vec{P}_B$ was fixed, and the laser power was used as a tuning or bifurcation parameter. Note that the blue laser wavelength was close to the absorbance peak at 420 nm, enabling us to trigger the isomerization and increase the amount of *cis* methyl red methyl ester isomer. There was no relevant temperature change in the DDLCC. The experiment was conducted at room temperature, approximately 20 °C. This meant that only an increase of the *cis*-isomer concentration was responsible for a decrease of birefringence on the liquid crystal. A Kepler telescope $K_B$ with a magnification of $\times 1/5$ was used to change the waist of the blue laser. The orientational molecular order in the dye-doped liquid crystal interacted with the blue light, making blue light sampling unsuitable for scanning the optical response of the liquid crystal sample.

To uncouple the excitation and probing fields, we provided illumination with a 532 nm Verdi V-2 polarized green laser as a probing light. Indeed, the absorbance at 532 nm is negligible for methyl red methyl ester, as seen in Figure 2. Both the green laser polarization $\vec{P}_G$ and its intensity were set fixed. A Kepler telescope with a magnification of $\times 2$ was used to expand the beam and obtain a more homogeneous illumination. A long-pass dichroic mirror DM (cutoff wavelength at 500 nm) was mounted in a pitch-yaw kinematic mount to

control the reflection angle and thus the position of the blue laser on the DDLCC. A second dichroic mirror was used to filter out the excitation light from the optical path to the 1/2" CCD camera. To record the images, a set of illumination optics was used to enhance the image quality. A first pair of lenses in a Kepler telescope configuration with an optical zoom of $\times 2$ and a secondary zoom lens with a magnification of $\times 7$ was used. This system allowed s to achieve diffractionless recordings on the elements in the DDLCC plane, ensuring no diffractive rings on the images were recorded. Likewise, we displaced the liquid crystal cell parallel to the optical axis with respect to the dichroic mirrors, and no changes were observed in the ring patterns. This guaranteed that the observed phenomenon was not diffractive in nature. Figure 1b shows the probing illumination field in the upper panel, and the lower panel shows both the excitation and probing fields obtained by the CCD camera, respectively. The dynamical behavior of the order parameter could not be completely sampled only by measuring the excitation field. A set of imagining lenses was used to enhance the recorded images. In particular, we used a $\times 2$ magnification telescope coupled with a zoom lens and density filters. Notice that both excitation and probe illuminations were collimated when reaching the DDLCC. Thus, diffractive effects induced by changes in the position along the optical axis of the DDLCC were negligible. This meant that the position of the DDLCC was not a parameter of the experiment. The dynamics of the *cis* concentration and nematic order parameter did not depend on the cell position along the $\hat{z}$ axis, which was the axis of light propagation on the dye-doped liquid crystal cell.

### 2.2. Synthesis and Preparation of Dye-Dopant and Liquid Crystal Mixture

Dye-dopant: The methylred methyl ester was obtained from a Fischer–Spier esterification between methyl red (Sigma-Aldrich Inc., St. Louis, MO, USA) and methanol (Merck). The methanol was used as a reagent and solvent at reflux for 6 h with sulfuric acid (Merck) as a catalyst [32]. The final compound was characterized by Fourier Transform Infrared Spectroscopy, and the purity was confirmed by thin layer chromatography. The absorption spectrum of methyl red methyl ester was measured by employing a Spectroquant Pharo 300 spectrometer with a 1 cm optical path quartz cuvette in dichloromethane (Merck) solutions. The absorption spectrum is reported in Figure 2b).

Mixture preparation: The 1 wt% mixture was prepared by weighing each component and dissolving them separately into dichloromethane. The solutions were combined and homogenized by sonicating for 5 min. The solvent was removed by slow evaporation at room temperature.

### 2.3. Light-Induced Ring Patterns

When the dye-doped liquid crystal cell was illuminated with a probing light, the monitoring CCD camera showed a homogeneous dark greenish color throughout the cell, as illustrated in the snapshot of Figure 3b at $t_0$. When applying the blue light beam, we observed that the illuminated area immediately began to transmit more light. Figure 3a illustrates how the total transmitted intensity measured in the green channel of the CCD camera ($\Delta I_g$) evolved over time with respect to the transmitted light without the blue light beam ($I_{g,0}$). The temporal evolution of the detected light intensity was characterized by growth and subsequent saturation. Figure 3a shows two regions in which the growth (region $I$) and saturation region ($II$) could be distinguished. In order to describe the growth and saturation process, we modeled it using the following expression: $\Delta I_g(t)/I_{g,0} = A(1 - e^{t/\tau})$, where $A = 2.79$ and $\tau = 55.71$ s. Namely, the establishment of the stationary ring pattern required a time period on the order of one minute.

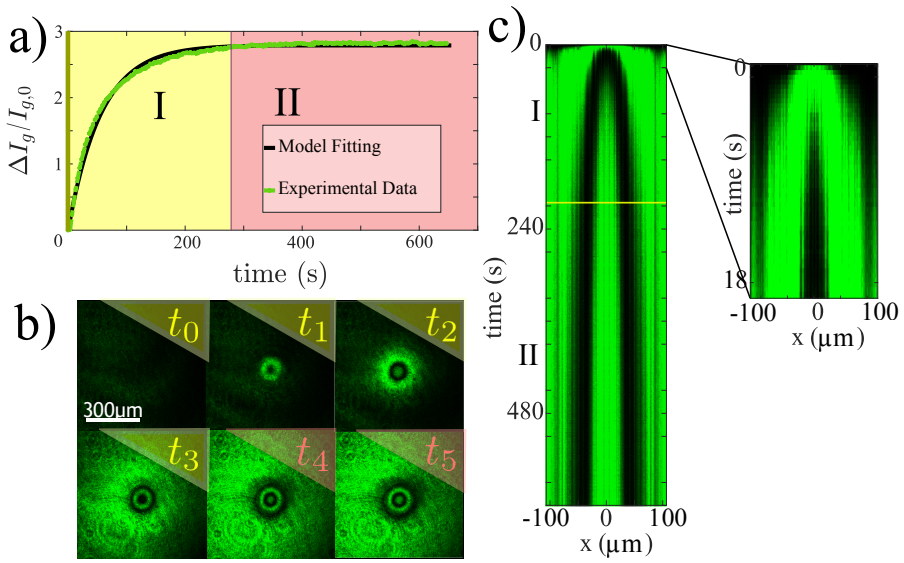


**Figure 3.** Experimental ring pattern emergence induced by a blue light (with a 445 nm wavelength) applied to a dye-doped liquid crystal cell, E7 NLC with azo-dye methyl red methyl ester at a concentration of 1 wt%. (**a**) Temporal evolution of transmitted total intensity, measured in the green channel of the CCD camera ($\Delta I_g$) with respect to the transmitted light without the blue light beam ($I_{g,0}$). The points were obtained experimentally, and the continuous curve was acquired using the expression $\Delta I_g(t)/I_{g,0} = A(1 - e^{t/\tau})$, where $A = 2.79$ and $\tau = 55.71$ s. Painted areas I and II account for the growth and saturation regions, respectively. (**b**) Temporal sequence of snapshots in the ring pattern formation process ($t_0 = 0$ s, $t_1 = 1$ s, $t_2 = 5$ s, $t_3 = 84$ s, $t_4 = 360$ s, and $t_5 = 570$ s). (**c**) Spatiotemporal diagram evolution of a diameter cut section.

When the blue light was applied, a region of light green with a darker center emerged; as time elapsed, this dark spot became a propagative ring. Note that the lightened region continued to grow, becoming even larger than the waist of the blue laser. Figure 1b compares the light green region to the waist size of the blue laser. As time continued to elapse, the dark ring continued to move away from the center, and a new dark spot emerged in the center, which then became a new dark ring. Figure 3b summarizes the temporal sequence of snapshots in the ring pattern formation process. In order to determine the process of spot emergence and ring propagation, we consider the spatiotemporal evolution of a diameter cut section. Figure 3c illustrates the observed spatiotemporal diagram evolution. From this chart, we see how the dark rings emerge, spread, and stop.

When we applied low powers of the blue laser (few mW, cf. Figure 4), the system did not show the formation of ring patterns, and we only observed the emergence of a light green spot. As the power was increased, this light green spot increased in size. With powers close to 40 mW, we began to observe the emergence of a dark spot in the center of the illuminated region (see Figure 4). Physically, we interpreted this region as a region of greater orientational disorder due to the consideration of the dye-doped liquid crystal sample between crossed polarizers. When we further increased the power of the blue laser, we observed the emergence of the first ring. Figure 4 shows the observed equilibrium ring. As the power increased, the diameter of the equilibrium ring grew. For powers close to 70 mW, we observed the emergence of a ring with a dark spot in the center as a state of equilibrium. As the power of the blue laser continued to increase, we observed that the central dark spot grew, and at a higher power, it became unstable, generating a new ring. Figure 4 summarizes the equilibria found for different blue laser powers.

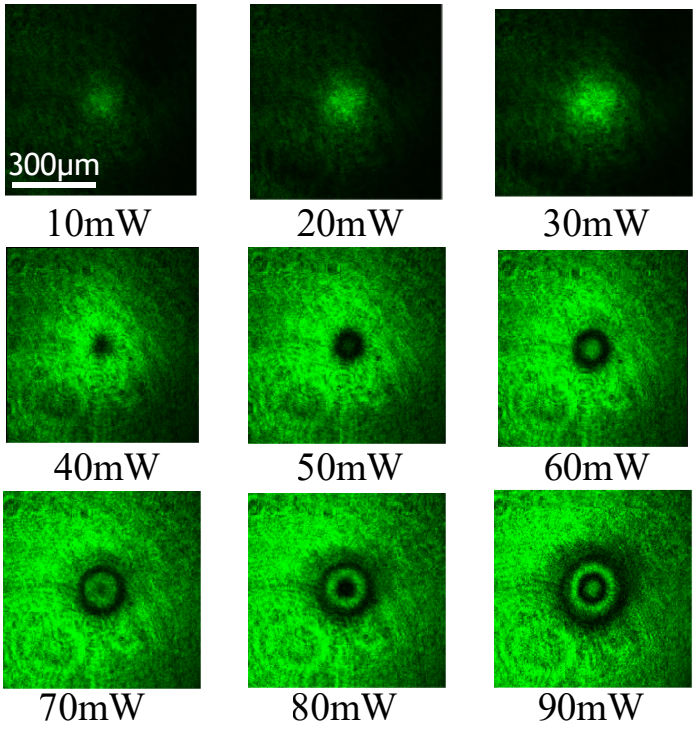


**Figure 4.** Equilibria ring patterns were experimentally observed for different powers of the blue light beam. After a long period of evolution, snapshots were observed for different powers, as denoted in the lower part of each snapshot.

## 3. Mathematical Modeling for Photo-Isomerization in Dye-Doped Liquid Crystals

Nematic liquid crystals are formed by rod-shaped molecules that—in a temperature range—can present an orientational rather than positional order. Then, the dynamics of the NLC can be described by a scalar order parameter $S(\vec{r};t)$ that accounts for the alignment of the molecules along a given direction [7–9], defined by

$$S(\vec{r};t) \equiv \frac{(3\langle\cos^2\theta\rangle - 1)}{2}, \tag{1}$$

where the brackets $\langle\cdot\rangle$ mean the spatial average in a microscopic element volume at position $\vec{r}$ and time $t$, and $\theta$ is the angle between the molecules and the local preferred direction [7–9]. Thus, $S$ accounts for the dispersion of the molecules with respect to their average direction. The scalar order parameter for a perfectly aligned nematic phase is $S = 1$, and that for an isotropic phase is $S = 0$. Note that a negative and large S shows that the molecules are oriented, but the choice of the current orientation does not coincide with the molecular average orientation. Close to a phase transition, Landau conjectured that the free energy can be written as a polynomial expansion of the order parameter [33]. Based on this type of approach, in the Landau–de Gennes theory, the transition between a nematic and an isotropic liquid state in a thin film is described by the dimensionless equation [7]

$$\partial_t S(r_\perp, t) = -AS + BS^2 - S^3 + \nabla^2 S, \tag{2}$$

where $r_\perp$ accounts for the transversal coordinate of the liquid crystal layer and $A$ is the bifurcation parameter, which is proportional to the difference between the current and critical temperature. Note that for large values of $A$, the isotropic state is favored in comparison to the nematic state. $B$ is a parameter that characterizes the size of the region of coexistence between the nematic and isotropic liquid state. The third and fourth terms on the right-hand side account for the nonlinear response of the medium and the spatial coupling of the order parameter, respectively. This coupling is diffusive in nature. Namely,

the flow of the order parameter is proportional to its gradient. This model predicts that the nematic and the isotropic liquid transition is of a subcritical nature. On the other hand, the concentration of molecules in the *cis*-state $C(\vec{r},t)$ at position $\vec{r}$ in time $t$ satisfies a relaxation and diffusion equation of the form [19]

$$\partial_t C = -\lambda[C - C_0(I)] + \delta\nabla^2 C, \tag{3}$$

where $\lambda$ is the decay rate related to the transition from a *cis* to *trans* state by thermal relaxation. $C_0(I)$ is the equilibrium concentration of molecules in the *cis* state that is proportional to the total intensity of the incident light $I$. Indeed, $C_0(I) \equiv \gamma I/(1+\eta I)$, where $\gamma$ and $\eta$ are dimensional parameters [19]. $\delta$ is the diffusion coefficient of the concentration of the *c*is state. As a result of the propagation of light, the intensity of the light has the following form:

$$I = I_0 e^{-r_\perp^2/w^2}, \tag{4}$$

where $w$ and $I_0$ are the light beam waist and the light intensity at the beam's center, respectively.

As we have mentioned, the incorporation of dye-dopants increases the nonlinear response of liquid crystals under the excitation of external fields [11,18–20,34]. Since the dye-dopant is not a liquid crystal and may even be immiscible, its excessive inclusion can prevent the mixture from being a liquid crystal; thus, a dye-dopant should be used in small amounts. We note that one of the reasons for considering methyl red methyl ester is that it is more miscible in E7 than other dopants; for example, methyl red. To describe the dynamics of the photo-isomerization process in the dye-doped nematic layer with planar anchoring, let us consider the concentration of molecules in the *cis*-state $C(\vec{r}_\perp,t)$ and the scalar order parameter $S(\vec{r}_\perp,t)$, which satisfy the dimensionless rate equations [21,22]

$$\begin{array}{rcl} \partial_t C &=& -\lambda[C - C_0(I) + \alpha S] + \delta\nabla^2 C + D\nabla^2 S, \\ \partial_t S &=& -(A+\beta C)S + BS^2 - S^3 + \nabla^2 S + D\nabla^2 C. \end{array} \tag{5}$$

The $\alpha$ parameter accounts for the reduction of the *cis*-state concentration when the liquid crystal molecules are more aligned (larger $S$) because the dye-dopants tend to be oriented in the direction of the molecules (transition from *cis* to *trans*) [19]. Indeed, the liquid crystal matrix tends to make the dye-dopants orient and stretch in the direction of the molecular order. The parameter $\beta$ stands for the entropic effect of the photo-isomerization process; that is, by increasing the concentration of the *cis* molecules, the disordered or non-oriented state is favored. Then, the linear term in S must decrease if the dye-dopant concentration increases. The parameter $D$ accounts for the mutual transport process; namely, a gradient in the dopant concentration induces the propagation of the order parameter [35].

In the limit of the large-scale separation between the order parameter S and the concentration of the *cis*-state ($\lambda \gg 1$) and for small $\alpha$ and intensity $I$, the cis-state concentration satisfies

$$C = C_0(I) \approx \gamma I = \gamma I_0 e^{-r_\perp^2/w^2}. \tag{6}$$

Therefore, the cis-state concentration acquires a Gaussian profile. Using this expression in the equation of the order parameter, $S$ satisfies the Landau–De-Gennes model for the nematic to isotropic transition induced by photo-isomerization [20]. Indeed, the bifurcation parameter $A(I) \equiv A + \beta\gamma I$ is controlled by the light intensity profile. When the sample is not illuminated, the system is in a NLC phase ($S_+$). When the sample is illuminated, the light can induce front propagation from the isotropic ($S_{IS}$) to the nematic phase [20].

### *3.1. Adiabatic Elimination and Effective Model*

To determine the dynamics described by Equation (5), one can consider the adiabatic elimination of the *cis*-state concentration [36]. Indeed, by assuming that the temporal evolution of the *cis*-state concentration is rapid compared to the dynamics of the order

parameter—i.e., $\lambda \gg 1$—and by using Neumann series, one can approach, in a dominant order, the *cis* concentration by

$$C \simeq C_0(I) - \alpha S + \frac{D - \alpha\delta}{\lambda}\nabla^2 S. \tag{7}$$

Introducing this expression in the equation for the order parameter S, at a dominant order, we obtain

$$\begin{aligned} \partial_t S &= -[A + \beta C_0(I)]S + (B - \alpha\beta)S^2 - S^3 + (1 - D\alpha)\nabla^2 S \\ &+ \frac{D(D - \alpha\delta)}{\lambda}\nabla^4 S + \frac{\beta}{\lambda}(D - \delta\alpha)S\nabla^2 S + D\nabla^2 C_0(I). \end{aligned} \tag{8}$$

Renormalizing the space $\vec{r} = \vec{r}'[\lambda/D(\delta\alpha - D)]^{1/4}$, the effective model reads

$$\partial_t S = -\tilde{A}S + \tilde{B}S^2 - S^3 - \nu\nabla^2 S - \nabla^4 S + bS\nabla^2 S + \tilde{\eta}, \tag{9}$$

where

$$\tilde{A}(\vec{r}') \equiv A + \beta C_0(I(\vec{r}')), \tag{10}$$

$$\tilde{B} \equiv (B - \alpha\beta), \tag{11}$$

$$\nu \equiv D\alpha - 1\sqrt{\frac{\lambda}{D(\delta\alpha - D)}}, \tag{12}$$

$$b \equiv \frac{\beta(D - \delta\alpha)}{\sqrt{\lambda D(\delta\alpha - D)}}, \tag{13}$$

$$\tilde{\eta}(\vec{r}') \equiv D\sqrt{\frac{\lambda}{D(\delta\alpha - D)}}\nabla^2 C_0(I). \tag{14}$$

The model in Equation (9) corresponds to a non variational Swift–Hohenberg-type equation [37,38]. This model has been used to study patterns [39,40], localized, stationary [37,41], and propagative structures [42,43], and spatiotemporal chaotic extended [40] and localized structures [44]. These phenomena have been studied in different contexts ranging from physics and chemistry to biology. The physical origin of the formation of spatial structures is due to the anti-diffusion coefficient ($\nu > 0$), which represents the different scales of the transport processes of the *cis* order and state parameter, which introduces an intrinsic characteristic scale: the Turing mechanism [45]. Namely, by having two transport processes with different scales, the system cannot propagate the order parameter and the *cis*-state homogeneously; thus, it self-organizes, forming patterns.

### *3.2. Homogeneous Illumination and Bifurcation Diagram*

Considering a spatially homogeneous illumination—that is, $C_0$ is a constant—the parameters that characterize the nematic and isotropic liquid transition are renormalized and independent of the space. The effective model has the form

$$\partial_t S = -\tilde{A}S + \tilde{B}S^2 - S^3 - \nu\nabla^2 S - \nabla^4 S + bS\nabla^2 S. \tag{15}$$

The homogeneous phases of this model have the form $S_0 = 0$ and

$$S_\pm = \frac{\tilde{B} \pm \sqrt{\tilde{B}^2 - 4\tilde{A}}}{2}, \tag{16}$$

where $S_0$ and $S_\pm$ account for the liquid isotropic and nematic phase. For high temperatures—i.e., a large $\tilde{A}$—it is expected that the only stable state is the isotropic liquid phase $S_0$. When decreasing $\tilde{A}$, the system presents a coexistence between the isotropic and nematic phase for $\tilde{A} = A_{sn} \equiv \tilde{B}^2/4$. This bifurcation occurs due to the emergence of two new equilibria:

the saddle-node bifurcation causes the emergence of a stable nematic state ($S_+$) and an unstable state ($S_-$). Figure 5 shows the bifurcation diagram of the model in Equation (15). As $\tilde{A}$ continues to decrease, the isotropic liquid state $S_0$ is as favorable as the nematic phase $S_+$ for $A = A_M \equiv 2\tilde{B}^2/9$—the Maxwell point [46]. Then, a flat wall between these two phase states at this critical point is characterized by being motionless. When further decreasing $\tilde{A}$, the isotropic liquid phase presents a spatial instability. We can study this instability by linearizing Equation (15) around the isotropic liquid state $S_0 = 0$, and considering the ansatz $S(\vec{r}, t) = S' e^{i\vec{k}\vec{r}+i\sigma t}$, we obtain the growth rate equation:

$$\sigma = -\tilde{A} + \nu\vec{k}^2 - \vec{k}^4, \tag{17}$$

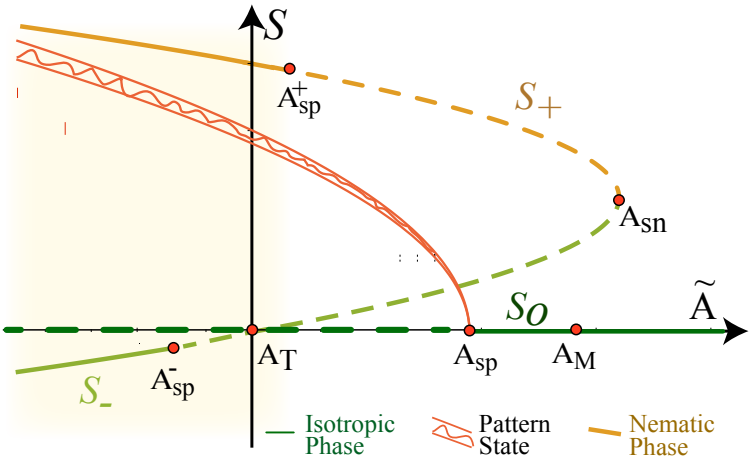


**Figure 5.** Schematic representation of the bifurcation diagram of the effective model in Equation (15) with constant coefficients. The order parameter $S$ as a function of the bifurcation parameter $\tilde{A}$. $S_0$, $S_+$, and $S_-$ account for the isotropic liquid and nematic phases, respectively. The continuous and dashed lines account for stable and unstable states respectively. $A_{sn}$, $A_M$, and $A_T$ are the critical points that account for the emergence of the nematic phase; both phases are equally favored, with a transcritical bifurcation of the isotropic liquid phase. $A_{sp}$, $A^+_{sp}$, and $A^-_{sp}$ account for the spatial instabilities of the homogeneous phases. The painted area shows the region of coexistence between the periodic state and the homogeneous state. The decorated curve explains the amplitude of the patterns.

The instability condition is $d\sigma(k_c)/dk = 0$ and $\sigma(k_c) = 0$. The first condition determines the critical length $k_c = \sqrt{\vec{k}^2} \equiv \sqrt{\nu/2}$, and the second defines the critical relation of the parameters for the spatial instability, which has the form $\tilde{A} = A_{sp} \equiv \nu^2/4$. Weakly nonlinear analysis shows that this instability is of a supercritical nature for a small $\tilde{B}$. Thus, despite the fact that the linear term is positive, $0 < \tilde{A} < A_{sp}$, the isotropic liquid state is unstable. For $\tilde{A} = A_T \equiv 0$, the system presents a transcritical bifurcation between unstable states.

To study the stability of the nematic phase, we use a similar strategy as in the study of the spatial stability of the isotropic liquid phase. Let us consider the linear perturbation $S = S_\pm + \chi$, where $\chi$ is a small variable that satisfies the equation

$$\partial_t\chi = (-\tilde{A} + 2\tilde{B} - 3S_\pm^2)\chi - (\nu + bS_\pm)\nabla^2\chi - \nabla^4\chi. \tag{18}$$

Introducing the ansatz $\chi(\vec{r}, t) = \chi' e^{i\vec{k}\vec{r}+i\sigma t}$ in the above equation, we obtain

$$\sigma = -\tilde{A} + 2\tilde{B} - 3S_\pm^2 + (\nu + bS_\pm)\vec{k}^2 - \vec{k}^4. \tag{19}$$

Imposing the spatial instability conditions, we obtain $k_c = \sqrt{\vec{k}^2} = \sqrt{(\nu + bS_\pm)/2}$ and

$$2\tilde{A} + \tilde{B}S_\pm = -\frac{(\nu + bS_\pm)^2}{4}. \tag{20}$$

From this expression, we obtain two critical conditions for spatial instability $A_{sp}^{+}$ and $A_{sp}^{-}$ corresponding to each of the nematic states (see Figure 5). Therefore, the effective model predicts a region of coexistence between a pattern state and a nematic phase. Figure 5 shows this region of coexistence with a painted area.

### *3.3. Light-Induced Ring Pattern*

Figure 5 summarizes the different behaviors presented by the model in Equation (15). From this chart, we conclude that the system has a coexistence region between the nematic state and the pattern. Note that this pattern alternates between areas of higher and lower orientation order [21,22]. This affects the sample's refractive index; therefore, if a light beam passes through the sample in a patterned state, one expects to observe interference fringes. As the light intensity increases, the bifurcation parameter $\tilde{A}$ grows. Then, if one considers a light intensity with a Gaussian profile, the parameter $\tilde{A}(I)$ is characterized by being inhomogeneous, with a bell-like shape. Thus, if the cell is in a nematic phase when the sample is illuminated, the central part of the light beam can induce the cell to leave the coexistence region, and only the pattern will be stable. For this type of region, we would expect to find that the illuminated area shows patterns because the central area of the light beam is circular, and for a small-waist beam, one would expect to see ring-like patterns. Figure 6 shows the typical equilibrium ring pattern observed numerically for the model Equation (9). All numerical simulations presented are obtained by considering finite differences coded with the Runge–Kutta order-4 algorithm.

If the system is not illuminated, $I_0 = 0$, the uniform nematic phase is the equilibrium of the system. By illuminating the system with a low intensity, we found numerically that there was a slight decrease in the reorientation order and an increase in the *cis* concentration in the central part of the Gaussian (cf. Figure 7). As the intensity $I_0$ increased, the size of the central spot showed greater orientation disorder; that is, the order parameter $S$ decreased in the central zone as $I_0$ increased. Note that the spot of the orientational disorder was smaller than the waist of the Gaussian forcing. As $I_0$ increased in the central zone, the parameter of order $S$ approached zero (isotropic liquid). When it hit zero, it generated a new dynamical behavior; the central point expanded, creating a ring. The origin of the clearing out of the central zone was due to the fact that the order parameter $S$ became negative. This could be interpreted as two ordered regions separated by a circular interface of the disordered state. A dark ring in Figure 7 represents this region. As $I_0$ increased further, the ring continued to expand. By further increasing the intensity of the Gaussian forcing, we observed the emergence of a new central spot surrounded by a ring. Note that for this parameter region, when beginning with a uniform nematic state and applying Gaussian forcing, a central spot of disorder state initially emerged that expanded, forming a ring that continued to propagate; later, another central spot of disorder state emerged, and finally the ring pattern stopped and remained in a stationary state. Experimentally, we observed a similar behavior to that observed numerically (see Figure 3). As the intensity of the Gaussian forcing $I_0$ increased further, new central spots emerged, which became new rings of disordered states (see Figure 7). The waist of the light beam limits the above process. This process is similar to the experimental process (see Figure 3).

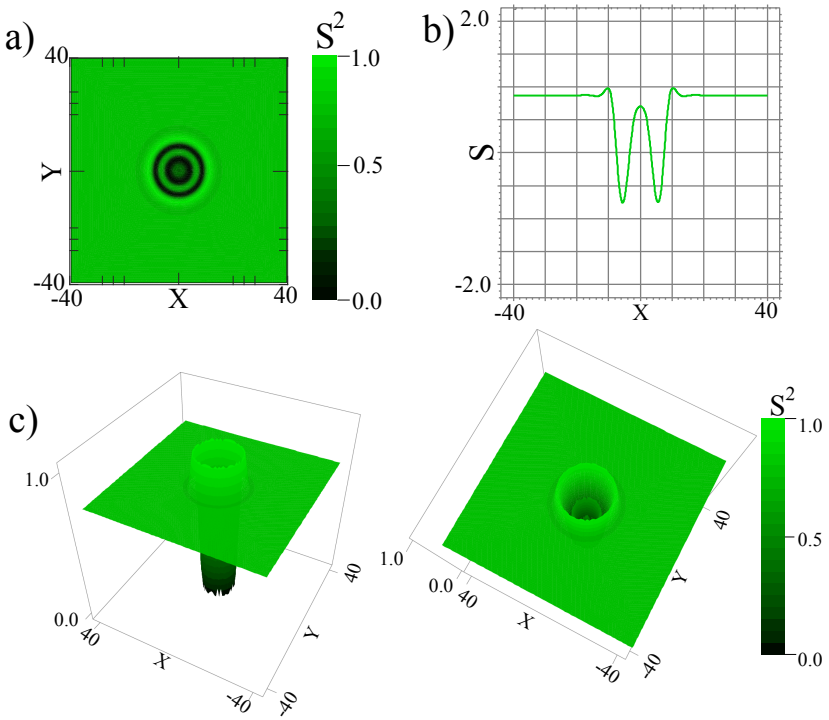


**Figure 6.** Numerical stationary ring pattern in a dye-doped nematic liquid crystal using the effective model in Equation (9) for $\tilde{A} = -0.5$, $\tilde{B} = 0.3$, $\nu = 1.05$, $b = 0.1$, $I_0 = 1.45$, and $w = 4$. (**a**) Contour plot of the squared order parameter $S$. (**b**) Profile of the cut of the order parameter $S$ in the diameter of the ring pattern. (**c**) Surface plot of the squared order parameter $S$.

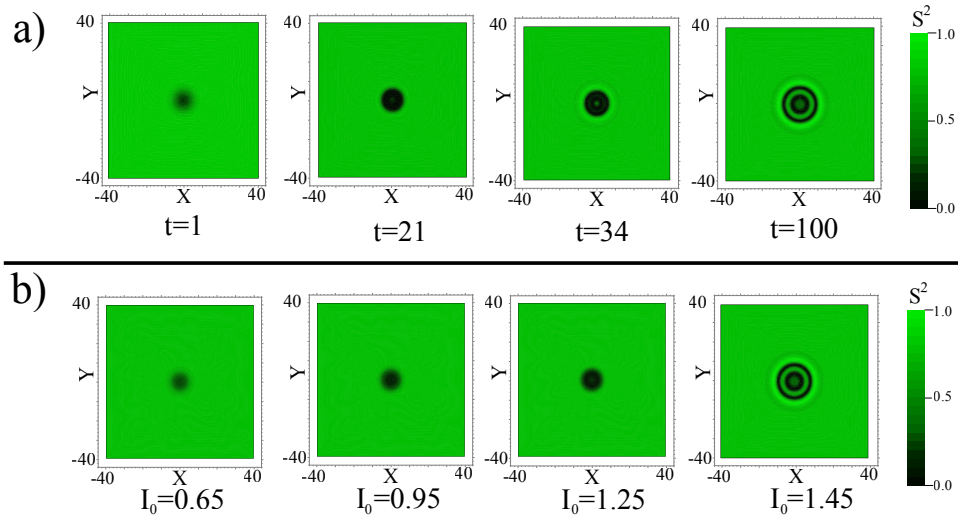


**Figure 7.** Numerical light-induced ring pattern in a dye-doped nematic liquid crystal using the model in Equation (9). (**a**) Temporal evolution of ring pattern using the effective model in Equation (9) for $\tilde{A} = -0.5$, $\tilde{B} = 0.3$, $\nu = 1.05$, $b = 0.1$, $I_0 = 1.45$, and $w = 4$. (**b**) Equilibrium of ring patterns numerically obtained for a different forcing strength $I_0$, and the other parameters are $\tilde{A} = -0.5$, $\tilde{B} = 0.3$, $\nu = 1.05$, $b = 0.1$, and $w = 4$.

In brief, the effective model in Equation (9) described the dynamics of the light-induced ring pattern in a dye-doped nematic liquid crystal well in qualitative terms.

## 4. Discussion

The emergence of ring patterns from an illuminated dye-doped nematic liquid crystal cell was initially attributed to the phase modulation of the diffractive light [27]. The light diffraction process is mathematically described by the nonlinear Schrödinger equation, which corresponds to the paraxial equation with a nonlinear correction associated with phase modulation. A local disturbance of the homogeneous state is characterized by the emergence of propagative rings towards the outside of the disturbance; these propagative rings are concentric with different thicknesses and decay with the square of the distance. In turn, the outer ring generates the emergence of outer rings with an increasingly smaller thickness. This type of pattern is similar to those reported for liquid crystal samples subjected to intense light rays [23]. The morphology of the ring pattern and the exhibited dynamics are different from those observed experimentally in the dye-doped nematic liquid crystal sample (see Figures 3 and 4).

The patterns found may allow manipulable interferometric patterns for light rays outside the absorption range of the dye-dopant. To illustrate the manipulability of the ring patterns, we adjusted the pitch and yaw of the dichroic mirror. Figure 8 schematizes the modification of the dichroic mirror, the effect on the light beam, and the observed ring patterns. Then, the light beam inside the doped liquid crystal sample could be shifted. Experimentally, we observed from the ring pattern in equilibrium that it moved almost rigidly. Figure 8b shows the light path scheme used and the ring patterns observed at the points marked on the path by discs. Likewise, it is important to note that the previous results showed that an interference mechanism does not cause the observed ring patterns. Note that the ring patterns caused by phase modulation were deformed with the angle of incidence [14], which is different from the observations in our setup (see Figure 8).

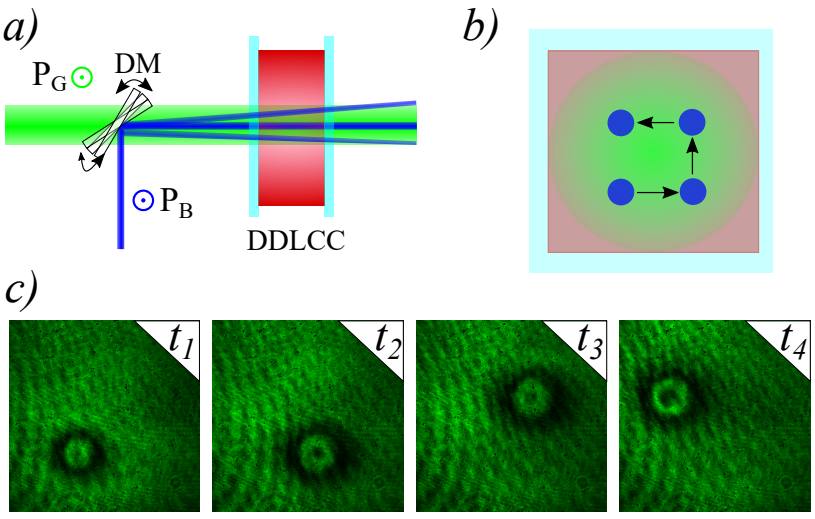


**Figure 8.** Manipulable ring patterns induced by illumination on a dye-doped liquid crystal sample. (**a**) Schematic representation of the mechanism for applying the light beam to the dye-doped liquid crystal sample. (**b**) Schematic representation of the path made by the light beam by adjusting the pitch and yaw of the dichroic mirror. (**c**) Snapshots of ring patterns observed at different times ($t_1 < t_2 < t_3 < t_4$).

## 5. Conclusions

Experimentally and theoretically, we have elucidated and characterized the origin of the ring patterns observed in a dye-doped nematic liquid crystal cell with planar anchoring under a light beam in the absorption band of the dye-dopant. To shed light onto the effect of the coherent excitation beam, we designed an experimental setup that considered two parallel beams—exciting and probing light—in which the probing light was monitored.

Based on a mathematical model that accounted for the coupling between the concentration of the *cis*-state and the orientational order parameter, we established the emergence of the rings as forming patterns in an inhomogeneous medium. Namely, the origin of the formation of pattern rings is due to the different scales and transport mechanisms of the concentration of the *cis*-state and the orientational order parameter. The formation of spatial structures induced by light can open up new applications such as the harnessing of diffraction gratings, masks, and irises. Work in this direction is in progress.

**Author Contributions:** Conceptualization, M.G.C. and G.G.-C.; methodology, G.G.-C., P.I.H., M.J.M. and J.V.; numerical analysis, L.A.L.; validation, G.G.-C. and L.A.L.; formal analysis, M.G.C. and L.A.L.; writing—original draft preparation, M.G.C.; improvement and verification of the manuscript, all authors. All authors have read and agreed to the published version of the manuscript.

**Funding:** This research was funded by FONDECYT grant number 1210353, the National Agency for Research and Development (ANID) Scholarship Program Becas Doctorado Nacional 2017211716, and ANID–Millennium Science Initiative Program-ICN17_012.

**Institutional Review Board Statement:** Not applicable.

**Informed Consent Statement:** Not applicable.

**Acknowledgments:** The authors acknowledge the fruitful discussions with Raouf Barboza.

**Conflicts of Interest:** The authors declare no conflict of interest.

## References

1. Newton, I. *Opticks, or, a Treatise of the Reflections, Refractions, Inflections & Colours of Light*; Sam. Smith and Benj. Walford, Printers to the Royal Society: London, UK, 1704.
2. Boyd, R.W. *Nonlinear Optics*; Academic Press: San Diego, CA, USA, 2003.
3. Shen, Y.R. *The Principles of Nonlinear Optics*; Wiley-Interscience: New York, NY, USA, 1984.
4. Mills, D.L. *Nonlinear Optics: Basic Concepts*; Springer Science & Business Media: Berlin/Heidelberg, Germany, 2012.
5. New, G. *Introduction to Nonlinear Optics*; Cambridge University Press: Cambridge, UK, 2011.
6. Lugiato, L.; Prati, F.; Brambilla, M. *Nonlinear Optical Systems*; Cambridge University Press: Cambridge, UK, 2015.
7. De Gennes, P.G.; Prost, J. *The Physics of Liquid Crystals*, 2nd ed.; Oxford Science Publications, Clarendon Press: Oxford, UK, 1993.
8. Chandrasekhar, S. *Liquid Crystal*; Cambridge University Press: New York, NY, USA , 1992.
9. Oswald, P.; Pieranski, P. *Nematic and Cholesteric Liquid Crystals*; CRC Press: Boca Raton, FL, USA, 2005.
10. Vertogen, G.; de Jeu, W.H. *Thermotropic Liquid Crystals, Fundamentals*; Springer Science & Business Media: Berlin/Heidelberg, Germany, 2012.
11. Khoo, I.C. *Liquid Crystals*; John Wiley & Sons: Hoboken, NJ, USA, 2007.
12. Takatoh, K.; Sakamoto, M.; Hasegawa, R.; Koden, M.; Itoh, N.; Hasegawa, M. *Alignment Technology and Applications of Liquid Crystal Devices*; CRC Press: Abingdon, UK, 2005.
13. Zel'Dovich, B.Y.; Pilipetskii, N.F.; Sukhov, A.V.; Tabiryan, N.V. Giant Optical Nonlinearity in the Mesophase of a Nematic Liquid Crystal. *JETP Lett.* **1980**, *31*, 263–267.
14. Zolot'ko, A.S.; Kitaeva, V.F.; Sobolev, N.K.N.; Chillag, L. The effect of an optical field on the nematic phase of the liquid crystal OCBP. *JETP Lett.* **1980**, *32*, 158–162.
15. Zolot'ko, A.S.; Kitaeva, V.F.; Sobolev, N.N.; Sukhorukov, A.P. Self-focusing of laser radiation in the course of the Fréedericksz transition in the nematic phase of a liquid crystal. *Zh. Eksp. Teor. Fiz.* **1981**, *81*, 933–941.
16. Durbin, S.D.; Arakelian, S.M.; Shen, Y.R. Optical-field-induced birefringence and Freedericksz transition in a nematic liquid crystal. *Phys. Rev. Lett.* **1981**, *47*, 1411–1414. [CrossRef]
17. Frisken, B.J.; Palffy-Muhoray, P. Electric-field-induced twist and bend Freedericksz transitions in nematic liquid crystals. *Phys. Rev. A* **1989**, *39*, 1513–1518. [CrossRef]
18. Khoo, I.C. Nonlinear optics of liquid crystalline materials. *Phys. Rep.* **2009**, *471*, 221–267. [CrossRef]
19. Jánossy, I.; Szabados, L. Photoisomerization of azo-dyes in nematic liquid crystals. *J. Nonlinear Opt. Phys.* **1998**, *7*, 539–551. [CrossRef]
20. Odent, V.; Clerc, M.G.; Falcón, C.; Bortolozzo, U.; Louvergneaux, E.; Residori, S. Photo-isomerization fronts in dye-doped nematic liquid crystals. *Opt. Lett.* **2014**, *39*, 1861–1864. [CrossRef]
21. Andrade-Silva, I.; Bortolozzo, U.; Clerc, M.G.; González-Cortés, G.; Residori, S.; Wilson, M. Spontaneous light-induced Turing patterns in a dye-doped twisted nematic layer. *Sci. Rep.* **2018**, *8*, 1–8. [CrossRef]
22. Andrade-Silva, I.; Bortolozzo, U.; Castillo-Pinto, C.; Clerc, M.G.; González-Cortés, G.; Residori, S.; Wilson, M. Dissipative structures induced by photoisomerization in a dye-doped nematic liquid crystal layer. *Phil. Trans. R. Soc. A* **2018**, *376*, 20170382. [CrossRef]

23. Durbin, S.D.; Arakelian, S.M.; Shen, Y.R. Laser-induced diffraction rings from a nematic-liquid-crystal film. *Opt. Lett.* **1981**, *6*, 411–413. [CrossRef]
24. Assanto, G. *Nematicons: Spatial Optical Solitons in Nematic Liquid Crystals*; John Wiley & Sons: Hoboken, NJ, USA, 2012.
25. Barnik, M.I.; Zolot'ko, A.S.; Kitaeva, V.F. Interaction of light with a dye-doped nematic liquid crystal. *J. Exp. Theor. Phys.* **1997**, *84*, 1122–1130. [CrossRef]
26. Deng, L.; He, K.; Su, W.; Sun, H.; Wang, R.; Zhang, H.; Liu, H.K. Optical limiting performances of the methyl-red-dye-doped nematic liquid crystal films. *Mater. Devices Syst. Disp. Lighting* **2002**, *4918*, 79–89.
27. Li, H.; Wang, J.; Wang, C.; Zeng, P.; Cai, P.; Pan, Y.; Yang, Y. Off-resonant nonlinear optical refraction properties of azo dye doped nematic liquid crystals. *Opt. Mater. Express* **2016**, *6*, 459–465. [CrossRef]
28. Serak, S.V.; Tabiryan, N.V.; Assanto, G. Nematicons in azobenzene liquid crystals. *Mol. Cryst. Liq. Cryst.* **2012**, *559*, 202–213. [CrossRef]
29. Park, H.S.; Oh, K.S.; Kim, K.S.; Chang, T.; Spiegel, D.R. Change of internal hydrogen bonding of methyl red upon photoisomerization monitored by Forced Rayleigh Scattering. *J. Phys. Chem. B* **1999**, *103*, 2355–2360. [CrossRef]
30. Castillo-Pinto, C.; Clerc, M.G.; González-Cortés, G. Extended stable equilibrium invaded by an unstable state. *Sci. Rep.* **2019**, *9*, 1–8. [CrossRef] [PubMed]
31. Kosa, T.; Sukhomlinova, L; Su, L.; Taheri, B.; White, T.J.; Bunning, T.J. Light-induced liquid crystallinity. *Nature* **2012**, *485*, 347–349. [CrossRef]
32. Kahl, D.J.; Hutchings, K.M.; Lisabeth, E.M.; Haak, A.J.; Leipprandt, J.R.; Dexheimer, T.; Khanna, D.; Tsou, P.S.; Campbell, P.L.; Fox, D.A.; et al. 5-Aryl-1,3,4-oxadiazol-2-ylthioalkanoic Acids: A Highly Potent New Class of Inhibitors of Rho/Myocardin-Related Transcription Factor (MRTF)/Serum Response Factor (SRF)-Mediated Gene Transcription as Potential Antifibrotic Agents for Scleroderma. *J. Med. Chem.* **2019**, *62*, 4350–4369. [CrossRef]
33. Landau, L.D.; Lifshitz, E.M. *Statistical Physics (Course of Theoretical Physics, Volume 5)*; Pergamon Press: New York, NY, USA, 1993.
34. Sasaki, T.; Ikeda, T. Photochemical switching of polarization in ferroelectric liquid crystals: Effect of structure of host FLCs. *Ferroelectrics* **1993**, *149*, 343–351. [CrossRef]
35. Bechhoefer, J.; Simon, A.J.; Libchaber, A.; Oswald, P. Destabilization of a flat nematic-isotropic interface. *Phys. Rev. A* **1989**, *40*, 2042–2056. [CrossRef] [PubMed]
36. Haken, H. *Synergetics: Introduction and Advanced Topics*; Springer: Berlin/Heidelberg, Germany, 1977.
37. Clerc, M.G.; Petrossian, A.; Residori, S. Bouncing localized structures in a liquid-crystal light-valve experiment. *Phys. Rev. E* **2005**, *71*, 015205. [CrossRef]
38. Kozyreff, G.; Tlidi, M. Nonvariational real Swift-Hohenberg equation for biological, chemical, and optical systems. *Chaos* **2007**, *17*, 037103. [CrossRef] [PubMed]
39. Kozyreff, G.; Chapman, S.J.; Tlidi, M. Interaction of two modulational instabilities in a semiconductor resonator. *Phys. Rev. E* **2003**, *68*, 015201. [CrossRef] [PubMed]
40. Clerc, M.G.; Verschueren, N. Quasiperiodicity route to spatiotemporal chaos in one-dimensional pattern-forming systems. *Phys. Rev. E* **2013**, *88*, 052916. [CrossRef]
41. Burke, J.; Dawes, J.H. Localized states in an extended Swift?Hohenberg equation. *SIAM J. Appl. Dyn. Syst.* **2012**, *11*, 261–284. [CrossRef]
42. Alvarez-Socorro, A.J.; Clerc, M.G.; Tlidi, M. Spontaneous motion of localized structures induced by parity symmetry breaking transition. *Chaos* **2018**, *28*, 053119. [CrossRef]
43. Houghton, S.M.; Knobloch, E. Swift-Hohenberg equation with broken cubic-quintic nonlinearity. *Phys. Rev. E* **2011**, *84*, 016204. [CrossRef]
44. Verschueren, N.; Bortolozzo, U.; Clerc, M.G.; Residori, S. Spatiotemporal chaotic localized state in liquid crystal light valve experiments with optical feedback. *Phys. Rev. Lett.* **2013**, *110*, 104101. [CrossRef]
45. Turing, A.M. The chemical basis of morphogenesis. *Philos. Trans. R. Soc. B* **1952**, *237*, 37–72.
46. Goldstein, R.E.; Gunaratne, G.H.; Gil, L.; Coullet, P. Hydrodynamic and interfacial patterns with broken space-time symmetry. *Phys. Rev. A* **1991**, *43*, 6700–6721. [CrossRef] [PubMed]